J|A|C|S
ARTICLES
Published on Web 05/02/2002

Iron Complexes Capped with Dendrimer-Appended Triazacyclononanes as the Novel Spatially Encumbered Models of Non-Heme Iron Proteins

Masashi Enomoto and Takuzo Aida*

Contribution from the Department of Chemistry and Biotechnology, Graduate School of Engineering, The University of Tokyo, 7-3-1 Hongo, Bunkyo-ku, Tokyo 113-8656, Japan

Received November 26, 2001

Abstract: Poly(benzyl ether) dendrimers with a 1,4,7-triazacyclononane (TACN) focal core (Ln_3TACN, **2a**−**4a**) and nondendritic L1_3TACN (**1a**), upon reaction with $FeCl_2$, followed by NaOAc and NH_4PF_6, afforded mononuclear iron(II) complexes $[Fe^{II}(\eta^2\text{-OAc})(Ln_3TACN)]^+$ (**1b**−**4b**), which were oxidized under O_2 to form dinuclear $(\mu\text{-O})(\mu\text{-OAc})_2$diiron(III) complexes (**1c**−**4c**) in 54−74% isolated yields. The formation of **1c**−**4c** obeyed second-order kinetics with respect to **1b**−**4b**, respecitvely, where the observed rate constants (k_2) were clearly dependent on the generation number of the dendritic substituents. Photoirradiation of **1c**−**4c** in the presence of NaOAc gave diiron(II) complexes (**1d**−**4d**), which were reoxidized to **1c**−**4c** by O_2, following first-order kinetics with respect to **1d**−**4d**, respectively. The crystal structure of nondendritic **1c** showed that the diiron(III) center is surrounded by an aromatic wall of the six 3,5-dimethoxybenzyl substituents, while spectroscopic profiles of dendritic **2c**−**4c** suggested that the geometries of their diiron(III) centers are little different from that of **1c**. The diiron(III) center of the largest **4c** was highly robust toward alkaline hydrolysis and also insulated electrochemically.

Introduction

Multinuclear metalloproteins are ubiquitous in the living cells, where non-heme metalloproteins with carboxylate-bridged diiron centers play important roles in dioxygen transportation and activation.[1] For example, hemerythrin, found in marine invertebrates, functions as an oxygen carrier through a redox cycle between the diiron(II) and diiron(III) oxidation states (Scheme 1).[2] Extensive studies have been made on synthetic diiron model complexes for understanding structural and electronic aspects of non-heme iron proteins.[1] However, in general, these model complexes are highly susceptible to hydrolysis and easily polymerized to give polynuclear complexes.[3] On the other hand, the diiron center of, e.g., hemerythrin is embedded in a hydrophobic region of the protein matrix and protected both hydrophobically and sterically from undesirable hydrolysis or polymerization.

Synthesis of diiron model complexes, so far reported, has made use of a "spontaneous self-assembly" of iron salts, carboxylato ligands, and capping ligands such as tris(1-pyrazolyl)hydroborate, tris(1-methylimidazol-2-yl)phosphine, and 1,4,7-triazacyclononane (TACN) derivatives.[1b] However, the self-assembling event is often accompanied by undesirable formation of chemically less active, doubly capped mononuclear iron complexes.[4] To overcome this problem and also to mimic natural systems more closely, use of bulky capping ligands bearing *tert*-butyl groups has been examined, whose diiron complexes, however, are thermodynamically labile and very likely to dissociate into mononuclear iron complexes with single capping ligands.[5] On the other hand, such mononuclear complexes are structurally related to the active centers of, e.g., iron superoxide dismutase,[6] tyrosine hydroxylase,[7] and catechol dioxygenase, and their structure−reactivity correlations have also attracted some attention.[8] Thus, capping ligands play important roles in structures and properties of model iron complexes of non-heme metalloproteins.[9]

Scheme 1. Reversible O_2-Binding at the Active Center of Hemerythrin

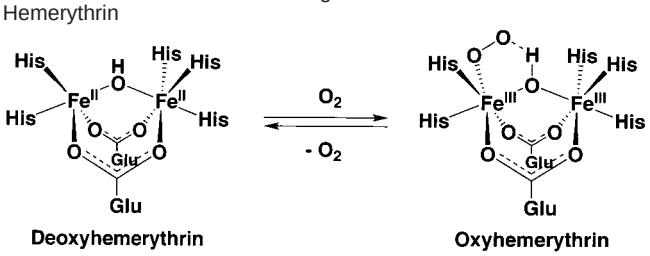

* Corresponding author. Fax: +81-3-5841-7310. E-mail: aida@macro.t.u-tokyo.ac.jp.

(1) (a) Lippard, S. J. *Angew. Chem., Int. Ed. Engl.* **1988**, *27*, 344. (b) Kurtz, D. M., Jr. *Chem. Rev.* **1990**, *90*, 585 and the references therein. (c) Moro-oka, Y.; Fujisawa, K.; Kitajima, N. *Pure. Appl. Chem.* **1995**, *67*, 241.
(2) (a) Stenkamp, R. E. *Chem. Rev.* **1996**, *96*, 2625. (b) Stenkamp, R. E.; Sieker, L. C.; Jensen, L. H.; McCallum, J. D.; Sanders-Loehr, J. *Proc. Natl. Acad. Sci. U.S.A.* **1985**, *82*, 713.
(3) Taft, K. L.; Lippard, S. J. *J. Am. Chem. Soc.* **1990**, *112*, 9629.
(4) (a) Armstrong, W. H.; Spool, A.; Papaefthymiou, G. C.; Frankel, R. B.; Lippard, S. J. *J. Am. Chem. Soc.* **1984**, *106*, 3653. (b) Wieghardt, K.; Pohl, K.; Gerbert, W. *Angew. Chem., Int. Ed. Engl.* **1983**, *22*, 727.
(5) Hikichi, S.; Ogihara, T.; Fujisawa, K.; Kitajima, N.; Akita, M.; Moro-oka, Y. *Inorg. Chem.* **1997**, *36*, 4539.
(6) Friedovich, I. *Acc. Chem. Res.* **1982**, *15*, 200.
(7) Dix, T. A.; Bollag, G. E.; Domanico, P. L.; Benkovic, S. J. *Biochemistry* **1985**, *24*, 2955.
(8) Que, L., Jr. *Iron Carriers and Iron Proteins*; Loehr, T. M., Ed.; VCH: New York, 1989; p 467.

In the present paper, we report a novel artificial model of non-heme iron proteins, whose metal ion center is encapsulated by a poly(benzyl ether) dendrimer cage. Dendrimers are nanosized, well-defined hyperbranched macromolecules with predictable three-dimensional shapes, and expected to serve as building blocks for organized functional materials.[10] Due to a gradient in branch density from the inner to the outer layers, large, spherical dendrimers eventually show unique conformational change dynamics, where the exterior termini are frozen to mobile because of their dense packing, while the interior core substantially retains its freedom of conformational motion.[11] Therefore, dendritic macromolecules at their center can provide a spatially isolated but less constrained nanoscopic void for the incorporation of certain functionalities,[10d] and are highly attractive as artificial substitutes for globular proteins.

We and other groups have reported iron complexes of dendrimer porphyrins,[12] which are capable of binding dioxygen in a reversible manner, due to a steric suppression of the μ-oxo dimer formation (bimolecular process) by the dendrimer framework. More recently, we have also reported the first example of a dendritic non-heme metalloprotein mimic by O_2-driven assembly of a copper-ligating dendrimer with a TACN focal core.[13] A mononuclear copper(I) complex of TACN bearing three-layered poly(benzyl ether) dendritic substituents (L3_3TACN, **3a**), upon exposure to O_2, spontaneously forms a dinuclear $[Cu^{III}_2(\mu\text{-}O)_2]^{2+}$ complex,[13] which is, in contrast with reported examples,[14] highly robust toward oxidative decomposition and can be regarded as a novel spatially encumbered model of hemocyanin and tyrosinase.

Here we report results of a study on application of such unique macromolecular ligands Ln_3TACN (*n* [number of the aromatic layers] = 1−4, **1a**−**4a**) to the exploration of bioinorganic chemistry of non-heme iron proteins. In particular, we should like to discuss structure−reactivity relationships and some mechanistic aspects of the oxygenation of iron(II) complexes capped with Ln_3TACN, together with "dendrimer effects" on chemical and electrochemical properties of the resulting iron(III) complexes.

Results and Discussion

Iron(II) Complexes of L*n*TACN (1b−4b) and Their Oxygenation. Lippard and co-workers have reported that a triazacyclononane (TACN) derivative such as trimethyl-TACN (Me$_3$TACN, **Me$_3$-1a′**) upon reaction with iron(II) salts followed by addition of NaOAc in an inert atmosphere affords an air-sensitive iron(II) complex, which adopts in the crystalline state a dinuclear form bearing two bridging OAc ligands and a μ-OH ligand $[(Fe^{II}_2(\mu\text{-}OH)(\mu\text{-}OAc)_2(Me_3TACN)_2)]^+$.[15] Oxygenation of this diiron(II) species results in the formation of $[Fe^{III}_2(\mu\text{-}O)(\mu\text{-}OAc)_2(Me_3TACN)_2]^{2+}$ (**Me$_3$-1c′**), which has been proposed to involve a sterically demanding "tetranuclear intermediate", by analogy to the oxidation of $[Fe^{II}(BIPhMe)_2(O_2CH)_4]$ (BIPhMe = 2,2′-bis(1-methylimidazolyl)phenylmethoxymethane) under O_2 (Scheme 2).[16] We investigated a similar sequence of the reactions using newly synthesized dendritic TACN derivatives **2a**−**4a** together with nondendritic **1a** (Chart 1) as capping ligands. For example, when L2_3TACN (**2a**) was allowed to react with $FeCl_2 \cdot 4H_2O$ in THF/MeCN under Ar, and then EtOH solutions of NaOAc and NH_4PF_6 were successively added to the reaction mixture, the colorless solution gradually turned yellow, to give an air-sensitive paramagnetic species (**2b**). However, in contrast with the case using **Me$_3$-1a′** as capping ligand,[15] **2b** did not show any vibrational bands at 3200−3800 cm^{-1}, characteristic of μ-OH in (μ-OH)(μ-OAc)$_2$diiron(II) species. On the other hand, upon bubbling with O_2, the solution gradually turned reddish brown, where the UV−vis spectrum showed new absorption bands at 352, 482, 525, and 722 nm typical of (μ-O)(μ-OAc)$_2$diiron(III) species.[17] Resonance Raman spectroscopy showed a band at 523 cm^{-1} due to symmetric Fe−O−Fe vibration (ν_{sym}), together with its combination with an Fe−N_{trans} stretching at 283 cm^{-1} and the first overtone at 1035 cm^{-1}. These spectral profiles, together with elemental analysis, indicate the formation of $[Fe^{III}_2(\mu\text{-}O)(\mu\text{-}OAc)_2(L2_3TACN)]^{2+}$ (**2c**) via oxygenation of **2b**. Use of other TACN derivatives such as **1a**, **3a**, and **4a**, in place of **2a**, for the above sequence of reactions also resulted in essentially the same spectroscopic profiles as those described above. After the mixtures were stirred overnight at 20 °C, binuclear complexes **1c**−**4c** were isolated

Scheme 2. Mechanism of the Oxidation of $[Fe^{II}(BIPhMe)_2(O_2CH)_4]$ (BIPhMe = 2,2′-bis-(1-methylimidazolyl)phenylmethoxymethane) under O_2, Involving a Sterically Demanding Tetranuclear Intermediate[16]

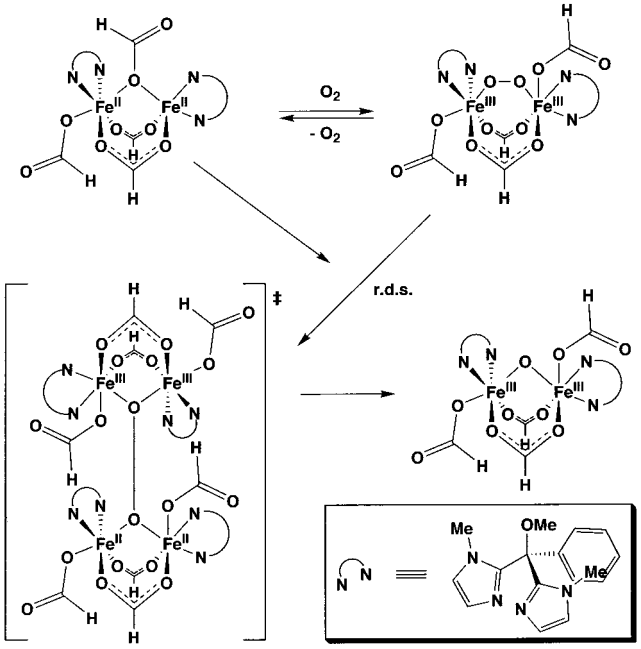

(9) (a) LeCloux, D. D.; Barrios, A. M.; Mizoguchi, T. J.; Lippard, S. J. *J. Am. Chem. Soc.* **1998**, *120*, 9001. (b) Ookubo, T.; Sugimoto, H.; Nagayama, T.; Masuda, H.; Saito, T.; Tanaka, K.; Maeda, Y.; Okawa, H.; Hayashi, Y.; Uehara, A.; Suzuki, M. *J. Am. Chem. Soc.* **1996**, *118*, 701.
(10) For recent reviews, see: (a) Zeng, F.; Zimmerman, S. C. *Chem. Rev.* **1997**, *97*, 1681. (b) Bosman, A. W.; Janssen, H. M.; Meijer, E. W. *Chem. Rev.* **1999**, *99*, 1665. (c) Vögtle, F.; Gerstermann, S.; Hesse, R.; Schwierz, H.; Windisch, B. *Prog. Polym. Sci.* **2000**, *25*, 987. (d) Hecht, S.; Fréchet, J. M. J. *Angew. Chem., Int. Ed. Engl.* **2001**, *40*, 74.
(11) (a) Jiang, D.-L.; Aida, T. *J. Am. Chem. Soc.* **1998**, *120*, 10895. (b) Hecht, S.; Fréchet, J. M. J. *J. Am. Chem. Soc.* **1999**, *121*, 4084.
(12) (a) Jiang, D.-L.; Aida, T. *Chem. Commun.* **1996**, 1523. (b) Jiang, D.-L.; Aida, T. *J. Macromol. Sci., Pure Appl.* **1997**, *A34*, 2047. (c) Collman, J. P.; Fu, L.; Zingg, A.; Diederich, F. *Chem. Commun.* **1997**, 193.
(13) Enomoto, M.: Aida, T. *J. Am. Chem. Soc.* **1999**, *121*, 874.
(14) Halfen, J. A.; Mahapatra, S.; Wilkinson, E. C.; Kaderli, S.; Young, V. G., Jr.; Que, L., Jr.; Zuberbühler, A. D.; Tolman, W. B. *Science* **1996**, *271*, 1396.
(15) Hartman, A. R.; Rardin, R. L.; Chaudhuri, P.; Pohl, K.; Wieghardt, K.; Nuber, B.; Weiss, J.; Papaefthymiou, G. C.; Frankel, R. B.; Lippard, S. J. *J. Am. Chem. Soc.* **1987**, *109*, 7387.
(16) Freig, A. L.; Masschelein, A.; Bakac, A.; Lippard, S. J. *J. Am. Chem. Soc.* **1997**, *119*, 334.
(17) See Supporting Information.

Chart 1

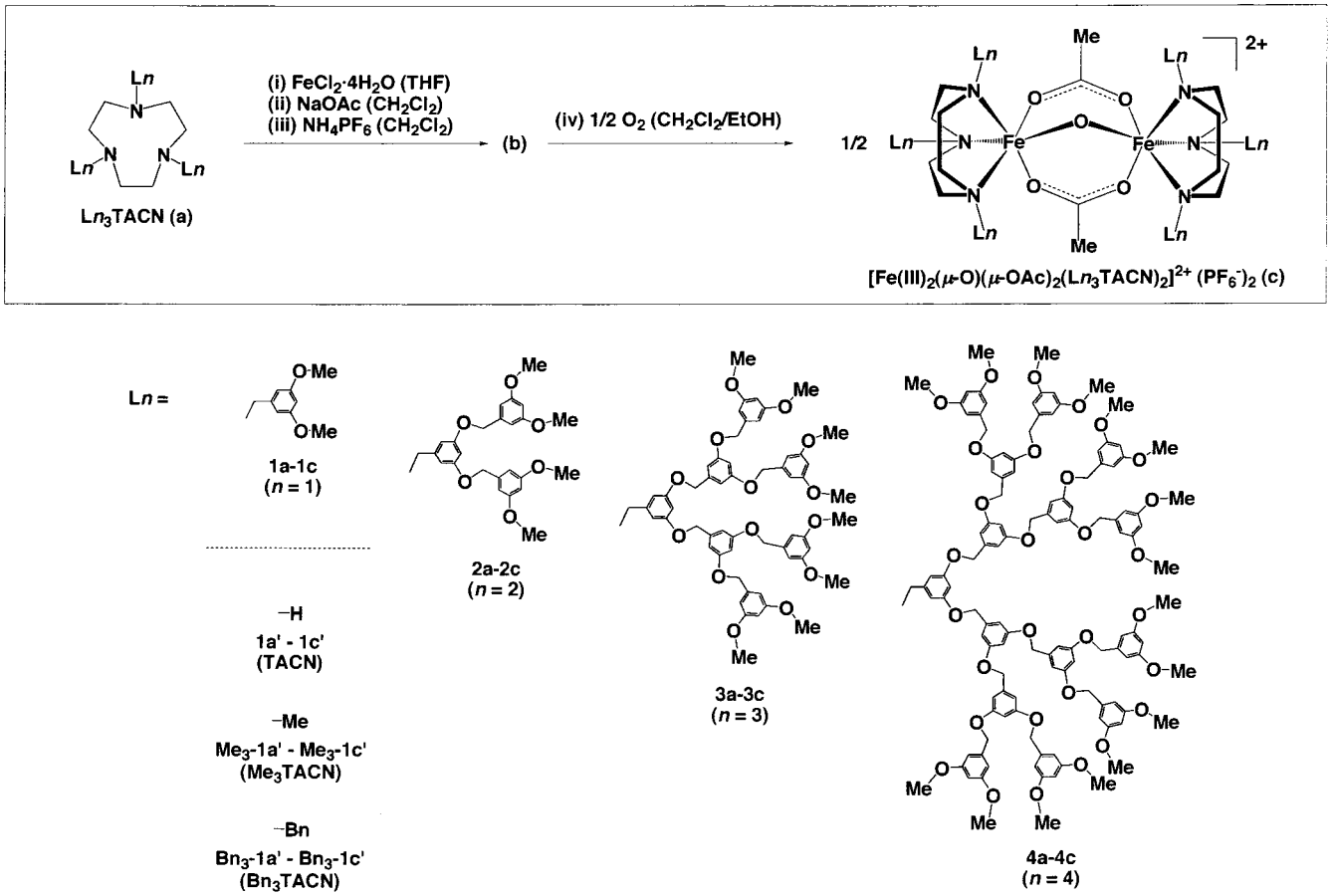

from the reaction mixtures in moderate to good yields [55% (**1c**), 54% (**2c**), 74% (**3c**), and 54% (**4c**, 48 h)] by means of crystallization or preparative SEC. This is rather interesting considering the large steric bulk of dendritic L*n*$_3$TACN, since oxo-bridged diiron(III) complexes have never been synthesized with bulky capping ligands carrying isopropyl or *tert*-butyl groups.[5]

Air-sensitive iron(II) complexes **1b**−**4b** most likely adopt a mononuclear form, which are oxidized under O_2 to form dinuclear complexes **1c**−**4c**, respectively. Size-exclusion chromatography (SEC, $CHCl_3$ as eluent) was informative of the structural aspects of these L*n*$_3$TACN-capped iron complexes. For example, $[Fe^{III}_2(\mu\text{-O})(\mu\text{-OAc})_2(L3_3TACN)]^{2+}$ (**3c**), prepared by exposure of **3b** to O_2, showed a unimodal, sharp SEC peak (Figure 1C) at a higher molecular weight region than free-base L3_3TACN (**3a**) (Figure 1A). On the other hand, when **3b** in Ar-purged $CHCl_3$ was directly subjected to SEC, the elution peak due to **3c** was only minor, whereas a lower molecular weight species with an elution volume similar to **3a** was observed predominantly (Figure 1B). UV−vis spectroscopy of this major fraction, isolated by SEC, showed a broad absorption band centered at 680 nm, which is obviously different from that of **3c** but typical of mononuclear iron(III) complexes.[5] In relation to these observations, when a mixture of **1b** and **3b** was exposed to O_2, an elution peak assignable to dinuclear $[Fe^{III}_2(\mu\text{-O})(\mu\text{-OAc})_2(L1_3TACN)(L3_3TACN)]^{2+}$ (**1**/**3c**) with two different TACN ligands was observed in addition to those of **1c** and **3c** (Figure 2A). On the other hand, a mixture of **1c** and **3c**, when allowed to stand under identical conditions to the above, did not show any sign of ligand scrambling in SEC (Figure 2B). It is likely that air-sensitive mononuclear complexes **1b**−**4b** have a fundamental structure $[Fe^{II}(\eta^2\text{-OAc})(L n_3TACN)]^+$, since a differential infrared spectrum of **2b**, obtained before and after the oxygenation,[17] showed vibrational bands at 1589 (ν_{asym}) and 1427 (ν_{sym}) cm^{-1} assignable to η^2-OAc,[18] which were converted under O_2 into two new bands at 1546 and 1392 cm^{-1}, characteristic of μ-OAc (**2c**), respectively.[18]

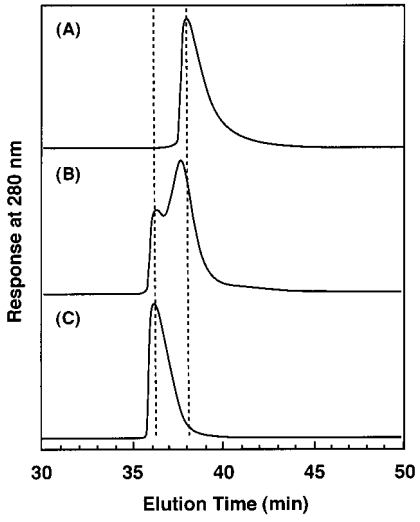

Figure 1. SEC profiles of (A) L3_3TACN (**3a**), (B) the iron(II) complex of L3_3TACN (**3b**) [oxidized during SEC], and (C) $[Fe^{III}_2(\mu\text{-O})(\mu\text{-OAc})_2(L3_3TACN)_2](PF_6)_2$ (**3c**).

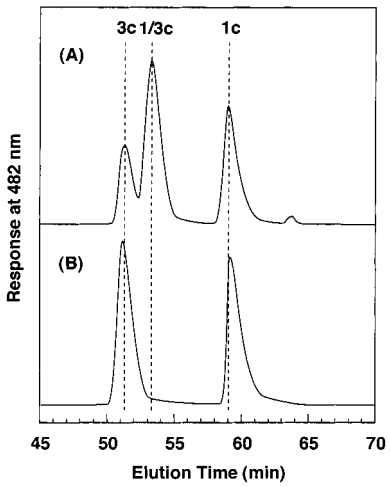

Figure 2. SEC profiles of (A) a mixture of iron(II) complexes **1b** and **3b** and (B) a mixture of $[Fe^{III}_2(\mu\text{-}O)(\mu\text{-}OAc)_2(L1_3TACN)_2](PF_6)_2$ (**1c**) and $[Fe^{III}_2(\mu\text{-}O)(\mu\text{-}OAc)_2(L3_3TACN)_2](PF_6)_2$ (**3c**), after being stirred under O_2 for 21 h at 20 °C in CH_2Cl_2/EtOH (3.75/1) containing NaOAc and NH_4PF_6. **1/3c**: $[Fe^{III}_2(\mu\text{-}O)(\mu\text{-}OAc)_2(L1_3TACN)(L3_3TACN)](PF_6)_2$.

Mechanistic Aspects of the Formation of (μ-O)(μ-OAc)$_2$Diiron(III) Complexes (1c−4c). Iron(II) complexes **1b**−**4b** are rare examples of TACN-appended mononuclear complexes. As expected, the transformation of **1b**−**4b** into **1c**−**4c** under O_2 depended significantly on the generation number of the dendritic substituents. For example, bubbling of a CH_2Cl_2/EtOH (3.75/1) solution of **3b** with O_2 at 20 °C resulted in a spectral change as shown in Figure 3A. Analysis of the spectral change profile indicated that the formation of **3c** obeys second-order kinetics with respect to **3b**.[17] Other iron(II) complexes such as **1b**, **2b**, and **4b**, in oxidation to the corresponding dinuclear iron(III) complexes, also showed second-order kinetics, where the observed rate constants (k_2) were clearly dependent on the generation number of the dendritic substituents (Figure 3B). In particular, k_2 of the largest **4b** (0.3×10^{-2} M^{-1} s^{-1}) was even one order of magnitude smaller than that of nondendritic **1b** (3.8×10^{-2} M^{-1} s^{-1}). The oxidation of mononuclear iron(II) complexes **1b**−**4b** under O_2 most likely occurs via (1) the initial binding of O_2 to the iron(II) center and (2) subsequent dimerization of the resulting dioxygenated complex with the remaining non-oxygenated complex to form a μ-peroxo-bridged species, which then undergoes (3) homolysis at the μ-peroxo bridge to form the diiron(III) complex (Scheme 3). The second-order kinetics for the formation of **1c**−**4c** indicates that step 2 is rate-determining, where a possible steric effect of the dendritic substituents must be pronounced.[19]

In relation to Scheme 3, when $^{18}O_2$ was used, in place of $^{16}O_2$, for the oxidation of **1b**, the resulting complex (**1c**) showed a broad Raman band centered at 517 nm,[17] whose second derivative profile showed two peaks at 500 and 520 nm. On the basis of the spectral profiles of related samples,[17] the former and latter bands are attributed to **[^{18}O]1c** ($[Fe^{III}_2(\mu\text{-}^{18}O)(\mu\text{-}OAc)_2(L1_3TACN)]^{2+}$) and **[^{16}O]1c** ($\nu_{sym}$, 20 cm^{-1} isotope shift), respectively. This observation clearly demonstrates that O_2 is directly incorporated into the oxidation sequence of **1b** to **1c** (Scheme 3). The formation of nonlabeled **[^{16}O]1c** suggests that some intermediate species, associated with the homolysis of the (μ-peroxo)diiron(III) complex (step 3), are highly subject to oxygen exchange with water, which in the present case most likely comes from the iron source ($FeCl_2 \cdot 4H_2O$), since **1c**−**4c**, including **Bn$_3$-1c′**, once formed no longer undergo oxygen exchange with water at the μ-oxo position, as described below. In fact, when a wet solvent containing few drops of $H_2{}^{18}O$ was used for the oxidation of **Bn$_3$-1b′** with $^{16}O_2$, the ^{18}O-labeled product at the μ-oxo position (**Bn$_3$-[^{18}O]1c′**) formed exclusively.[17]

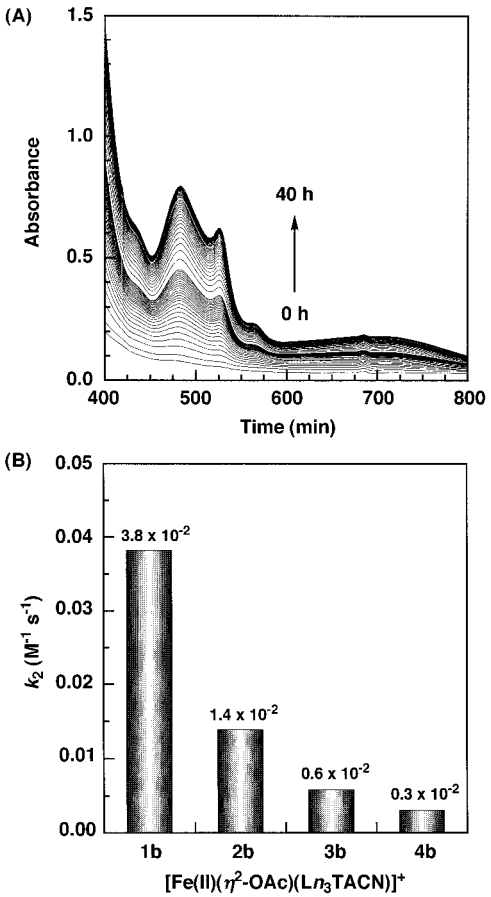

Figure 3. Reaction of **1b**−**4b** (7.9 mM) with O_2 in CH_2Cl_2/EtOH (3.75/1) at 20 °C in a quartz cell of 1 mm path length. (A) Absorption spectral change of **3b**. (B) Pseudo-second-order rate constants (k_2).

Photoreduction of (μ-O)(μ-OAc)$_2$Diiron(III) Complexes (1c−4c). In the course of the above study, we found a rather interesting phenomenon that (μ-O)(μ-OAc)$_2$diiron(III) complexes **1c**−**4c**, in the presence of NaOAc, are reduced by photoirradiation (>350 nm) to generate air-sensitive iron(II) species **1d**−**4d**, whose oxidation profiles are much different from those of **1b**−**4b**. For example, when a CH_2Cl_2/EtOH (5/1) solution of **4c**, in the presence of NaOAc, was irradiated under Ar with a xenon arc light through a UV cutoff filter (>350 nm), the characteristic absorption bands started to decay with time to give a pale yellow solution. A differential FT-IR spectrum of **2c**, obtained before and after the photoirradiation,[17] showed the appearance of vibrational bands at 1609 and 1425 cm^{-1} at the expense of those at 1546 and 1392 cm^{-1} due to μ-OAc of **2c**. On the other hand, when the solution was exposed to O_2, the absorption spectrum reverted to that of **4c** completely in 240 min (Figure 4A), indicating that the photoreduced species (**4d**) contains iron(II). The oxidation took place much more

(18) Deacon, G. B.; Phillips, R. J. *Coord. Chem. Rev.* **1980**, *33*, 227.
(19) A broad absorption band centered at 600 nm, assignable to a (μ-peroxo)-diiron(III) species, was observed in an early stage of the reaction after exposure to O_2.

Scheme 3. A Proposed Mechanism for the Oxidation of $[Fe^{II}(\eta^2\text{-OAc})(Ln_3TACN)]^+$ [**1b**−**4b** ($n = 1-4$)] under O_2, Involving a (μ-Peroxo)diiron(III) Intermediate

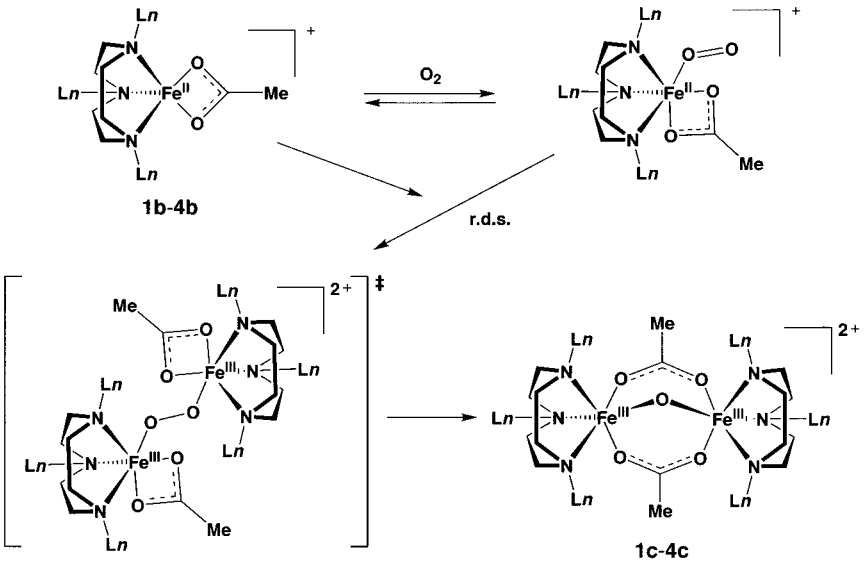

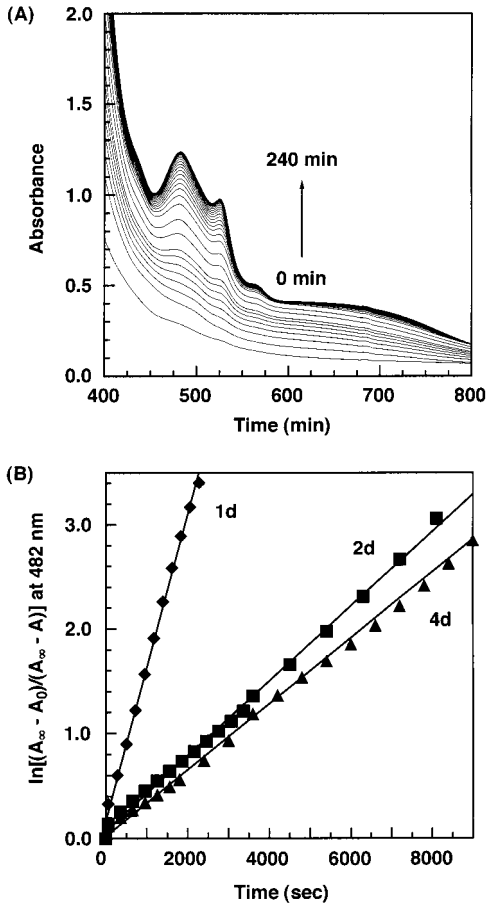

Figure 4. Reaction of photoreduced diiron(II) species **1d**, **2d**, and **4d** (4.17 mM) with O_2 in CH_2Cl_2/EtOH (5/1) at 30 °C in a quartz cell of 1 mm path length. (A) Absorption spectral change of **4d**. (B) First-order plots of absorption spectral changes of **1d**, **2d**, and **4d** at 482 nm.

rapidly than that of mononuclear **4b**, which required 40 h for completion (for one generation smaller **3b**, see Figure 3A). When **3c** was photoreduced in the presence of a spin trapping reagent such as α-phenyl-*N*-*tert*-butylnitrone (PBN), under otherwise identical conditions to the above, two different EPR-active species **I** [14.4 (A_N)/2.83 G (A_H)] and **II** [15.5 (A_N)/4.81 G (A_H)] were generated,[17] which are assignable to PBN adducts with acetoxy and methyl radicals, respectively.[20] This observation indicates the occurrence of one-electron oxidation of acetate ion to give acetoxy radical, which immediately decomposes to generate methyl radical and CO_2. Quite interestingly, analysis of the absorption spectral change profile (Figure 4A), upon reoxidation of **4d** under O_2, showed that the formation of **4c** obeys first-order kinetics with respect to **4d** (Figure 4B), where the observed rate constant (k_1) of 3.0×10^{-4} s^{-1} is not so much different from those with two-generation smaller **2d** (3.5×10^{-4} s^{-1}). From these observations, the photoreduced species is most likely a diiron(II) complex (Scheme 4), taking into account also the fact that a mixed-valence iron(II,III) species, a possible candidate, has been reported to be deep green in solution.[15] Thus, the oxygenation of the photoreduced species possibly results

Scheme 4. Proposed Mechanisms for Photoreduction of $[Fe^{III}_2(\mu\text{-O})(\mu\text{-OAc})_2(Ln_3TACN)_2]^+$ [**1c**−**4c** ($n = 1-4$)] and Re-oxidation of the Resulting Diiron(II) Complexes [**1d**−**4d** ($n = 1-4$)] under O_2, Involving a Diacetato-Bridged (μ-Peroxo)diiron(III) Intermediate

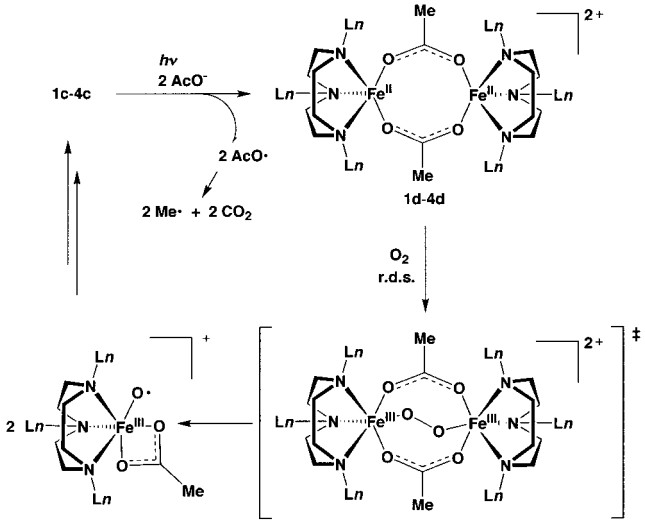

(20) Photolysis of $Hg(OAc)_2$ in the presence of PBN has been reported to give acetoxy and methyl radicals with *A*-values (G) in C_6H_6 of 12.97 (A_N)/1.82 (A_H) and 14.20 (A_N)/3.45 (A_H), respectively. Janzen, E. G.; Blackburn, B. J. *J. Am. Chem. Soc.* **1969**, *91*, 4481.

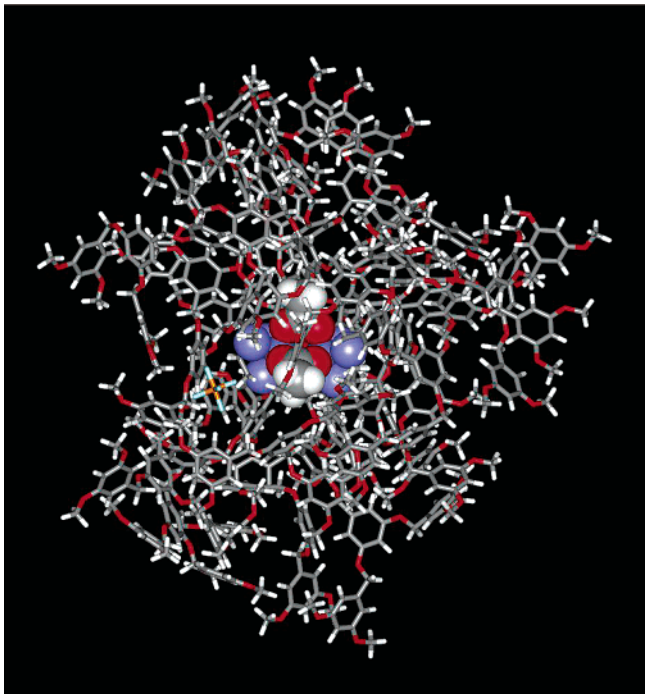

Figure 5. A computer-generated molecular model of $[Fe^{III}_2(\mu\text{-O})(\mu\text{-OAc})_2(L4_3TACN)_2](PF_6)_2$ (**4c**), optimized by a MM2 calculation with the CAChe software package (Oxford Molecular Ltd.), using the crystallographically defined geometry of **1c** (Figure 6) for the diiron(III) center.

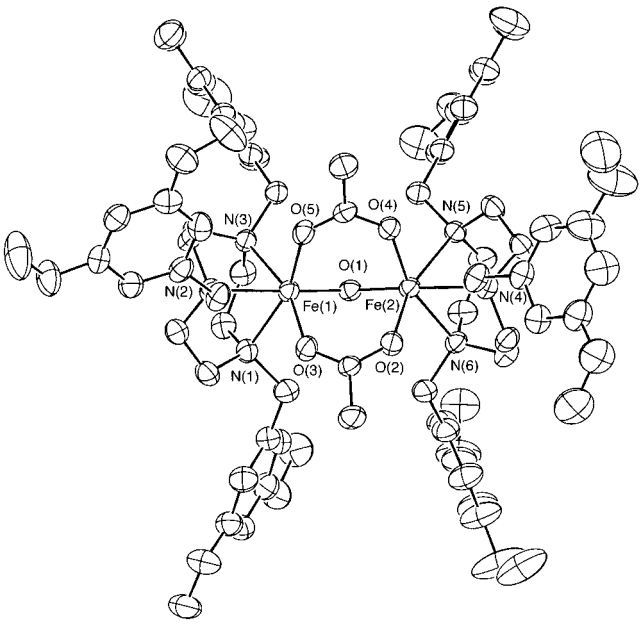

Figure 6. Crystal structure of $[Fe^{III}_2(\mu\text{-O})(\mu\text{-OAc})_2(L1_3TACN)_2](PF_6)_2$ (**1c**), showing 50% probability thermal ellipsoids. PF_6^- and hydrogen atoms are omitted for clarity.

in (1) transient formation of the corresponding (μ-peroxo)diiron(III) intermediate and (2) subsequent homolysis at the peroxo bridge followed by (3) recombination of the resulting highly reactive mononuclear iron(III)-O$^\bullet$ species to furnish the (μ-O)(μ-OAc)$_2$diiron(III) complex (Scheme 4). In the absence of acetate ion, the photoreduction proceeded sluggishly to give, after reoxidation under O_2, several unidentified products.

In relation to the above mechanism, we investigated photoreduction of a mixture of **1c** and **3c**, followed by reoxidation with O_2. If the reoxidation process actually involves dissociation of the (μ-peroxo)diiron(III) intermediate into the iron(III)-O$^\bullet$ species, ligand-scrambled **1**/**3c** must be formed in addition to original **1c** and **3c**. On the other hand, if the (μ-peroxo)diiron(III) intermediate is transformed without dissociation into the (μ-O)(μ-OAc)$_2$diiron(III) species as in Scheme 2, no ligand-scrambled product must be formed. In conformity with the proposed mechanism in Scheme 4, the SEC profile after reoxidation[17] clearly showed an elution peak due to **1**/**3c** between those of parent **1c** and **3c**. The first-order kinetics for the formation of the (μ-O)(μ-OAc)$_2$diiron(III) species (Figure 4B) may suggest that the binding of O_2 to the diiron(II) center is rate determining in the reaction presented in Scheme 4. The much faster oxidations of **1d**−**4d** than **1b**−**4b**, respectively, likely indicate a "pre-organization effect", which is characteristic of enzymatic reactions.

Structural Aspects of (μ-O)(μ-OAc)$_2$Diiron(III) Complexes (1c−4c). Figure 5 shows a computer-generated image of the largest **4c**, in which the diiron(III) center is completely encapsulated by the large dendrimer cage. Therefore, it is also interesting to investigate how the dendritic substituents affect the structure of the (μ-O)(μ-OAc)$_2$diiron(III) center. We successfully obtained a single crystal (reddish brown, rectangular shape) of **1c** by slow diffusion of ether vapor into a CH_2Cl_2 solution of **1c** at room temperature. As shown by an ORTEP diagram of the complex (Figure 6), the iron atoms adopt a distorted octahedral coordination geometry with a N_3O_3 ligand donor set, which are connected together by an oxo group and two OAc ligands between the cofacially oriented TACN caps. The dimethoxybenzyl units appear to form a sterically encumbered pocket to accommodate the diiron center. Although the core geometry of **1c** is similar to those reported for $[Fe^{III}_2(\mu\text{-O})(\mu\text{-OAc})_2(TACN)_2]^{2+}$ (**1c′**) and $[Fe^{III}_2(\mu\text{-O})(\mu\text{-OAc})_2(Me_3TACN)_2]^{2+}$ (**Me$_3$-1c′**), there are some deviations in structural parameters: The Fe−N$_{cis}$ and Fe−N$_{trans}$ bonds (average lengths = 2.212 and 2.280 Å, respectively) are longer than those of **1c′** (2.166 and 2.205 Å) and **Me$_3$-1c′** (2.198 and 2.217 Å). Furthermore, the average Fe−O (μ-oxo) bond (1.805 Å) is also slightly longer than those of **1c′** (1.781 Å) and **Me$_3$-1c′** (1.800 Å). Consequently, **1c** has the longest Fe···Fe distance (3.1442(7) Å) and the largest Fe−O−Fe angle (121.1(1)°) among the diiron/TACN complexes so far reported.[21,22] Accordingly, the absorption band of **1c** in MeOH at 351 nm, characteristic of (μ-O)diiron(III) complexes, was red shifted from those of **1c′** (335 nm) and **Me$_3$-1c′** (345 nm).[23] Furthermore, resonance Raman spectroscopy of a KCl pellet sample of **1c**, upon excitation at 532 nm, showed an Fe−O−Fe symmetric vibration (ν_{sym}) at 514 cm^{-1} (Figure 7A), which is obviously lower than those of **1c′** (540 cm^{-1}) and **Me$_3$-1c′** (537 cm^{-1}). This tendency falls in line with an increase in the Fe−O−Fe angle from **1c** (121.1(1)°) to **Me$_3$-1c′** (119.7(1)°) to **1c′** (118.7(4)°).[24] On the other hand, when dendritic **2c**−**4c** were compared with nondendritic **1c**, their UV−vis absorption[17] and resonance Raman spectral profiles (Figure 7B−D) were little different from that of nondendritic **1c**. For example, the largest **4c** in $CHCl_3$ showed a major absorption band due to the core unit at 352 nm, which

(21) Spool, A.; Williams, I. D.; Lippard, S. J. *Inorg. Chem.* **1985**, *24*, 2156.
(22) Wieghardt, K.; Pohl, J.; Ventur, D. *Angew. Chem., Int. Ed. Engl.* **1985**, *24*, 392.
(23) Reem, R. C.; McCormick, J. M.; Richardson, D. E.; Devlin, F. J.; Stephens, P. J.; Musselman, R. L.; Solomon, E. I. *J. Am. Chem. Soc.* **1989**, *111*, 4688.
(24) Sanders-Loehr, J.; Wheeler, W. D.; Shiemke, A. K.; Averill, B. A.; Loehr, T. M. *J. Am. Chem. Soc.* **1989**, *111*, 8084.

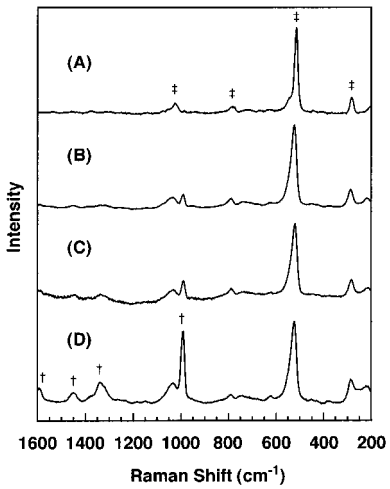

Figure 7. Resonance Raman spectra of $[Fe^{III}_2(\mu\text{-O})(\mu\text{-OAc})_2(Ln_3TACN)_2](PF_6)_2$ [**1c**−**4c** ($n = 1-4$)]. Peaks labeled with ‡ and † are due to diiron(III) center and dendrimer units, respectively.

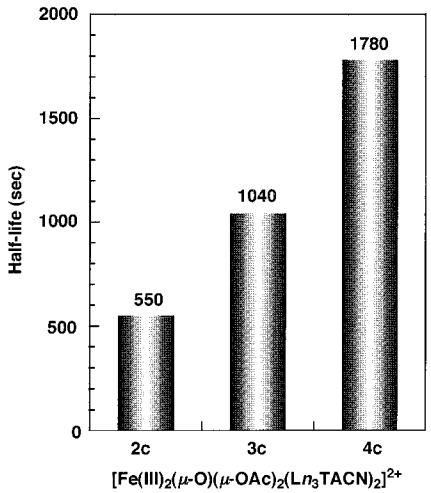

Figure 8. Half-lives of $[Fe^{III}_2(\mu\text{-O})(\mu\text{-OAc})_2(Ln_3TACN)_2](PF_6)_2$ [**2c**−**4c** ($n = 2-4$); 0.12 mM] at 50 °C in THF/H_2O (2.0/0.2 mL) in the presence of triethanolamine (76.2 mM).

is virtually identical with that of **1c** (351 nm).[17] Likewise, the ν_{sym} (Fe−O−Fe) frequency of **4c** (523 cm^{-1}) was only slightly higher than that of **1c** (514 nm). Thus, the structural parameters of the diiron(III) center are virtually intact to the generation number of the dendritic substituents. Poly(benzyl ether) dendrimers are rather flexible, so that the TACN-core dendritic ligands (Ln_3TACN) can eventually change their shape from globular to conical. Therefore, the diiron(III) center, even when attached to the largest $L4_3TACN$, is able to adopt an almost identical coordination geometry to that of **1c** without any significant structural distortion.

Hydrophobic Protection of Diiron(III) Center. In contrast with the case of non-heme diiron proteins,[25] the bridging oxo groups in artificial model complexes [(μ-O)(μ-$OAc)_2$diiron(III)] are known to be easily exchanged with ^{18}O in the presence of ^{18}O-labeled water ($H_2{}^{18}O$).[4a,21] For example, when **1c′** (3.75×10^{-2} mmol) was dissolved in MeCN (5 mL) containing 100 μL of $H_2{}^{18}O$, a Raman band due to Fe−^{16}O−Fe at 540 cm^{-1} gradually disappeared to give a new band due to Fe−^{18}O−Fe at 523 cm^{-1}. This exchange reaction proceeded fairly rapidly even at 30 °C with a concomitant decomposition of the (μ-$O^{16/18}$)(μ-$OAc)_2$diiron(III) complex. On the other hand, **2c**−**4c** under identical conditions to the above showed neither any sign of ^{18}O-exchange nor decomposition even after 5 days, where the intensity of the Raman band due to Fe−^{16}O−Fe remained unchanged. Further studies revealed that such an unusual stability of the diiron center is not only the case for dendritic **2c**−**4c** but could also be observed for a nondendritic (μ-^{16}O)(μ-$OAc)_2$diiron(III) complex capped with tribenzyl-TACN (**Bn_3-1c′**). Considering also the X-ray crystal structure of **1c**, the (μ-O)(μ-$OAc)_2$diiron(III) centers in **1c**−**4c** are hydrophobically protected against access of water, irrespective of the size of the dendron substituents. In contrast with the above case, **1c** decomposed rapidly in the presence of basic compounds. For example, when a THF solution of triethanolamine (3.35 M, 50 μL) was added at 50 °C to a THF solution (2.0 mL) of **1c** (0.12 mM) containing 200 μL of water, the characteristic 350 nm absorption band of **1c** disappeared completely within only 10 s. On the other hand, although dendritic **2c**−**4c** also decomposed under similar basic conditions, their decomposition rates were obviously much smaller than that of **1c**, and dependent on the generation number of the dendritic substituents (Figure 8). The largest **4c** (Figure 5) showed a half-life of 1780 s, which is more than 3 times longer than that of two-generation smaller **2c** (550 s). Therefore, the dendritic substituents on the TACN ligands serve as a barrier to protect the diiron(III) center from hydrolytic decomposition.

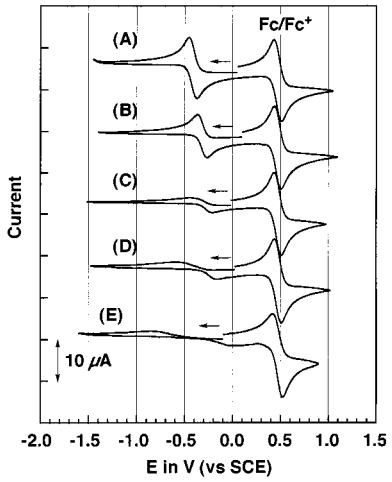

Figure 9. Cyclic voltammograms of $[Fe^{III}_2(\mu\text{-O})(\mu\text{-OAc})_2(Ln_3TACN)_2](PF_6)_2$: (A) **$Me_3$-1c′**, (B) **1c**, (C) **2c**, (D) **3c**, and (E) **4c** (1.0×10^{-3} mM) with a scan speed of 100 mV s^{-1} in MeCN containing Bu_4NPF_6 (0.2 M). Ferrocene was used as internal reference.

Electrochemical Insulation of Diiron(III) Center. Redox activities of **1c**−**4c** and **Me_3-1c′** as a reference were investigated by cyclic voltammetry in dry MeCN (Figure 9). Over a range from +1.5 to −2.0 V versus SCE, nondendritic **1c** clearly displayed a quasireversible wave at −0.319 V (Figure 9A), which is positive by 96 mV from that of **Me_3-1c′** (−0.415 V). On the other hand, when the dendritic substituents on the TACN ligands became larger from **1c** to **4c**, the redox potential ($E_{1/2}$) of the interior diiron(III) center turned more negative from −319 to −393 mV (vs SCE), and the voltage difference (ΔE) between the reduction and return oxidation peaks became larger. These results indicate that a diiron(III) complex bearing larger dendritic

(25) (a) Shiemke, A. K.; Loehr, T. M.; Sanders-Loehr, J. *J. Am. Chem. Soc.* **1984**, *106*, 4951. (b) Shiemke, A. K.; Loehr, T. M.; Sanders-Loehr, J. *J. Am. Chem. Soc.* **1986**, *108*, 2437.

ligands is more reluctant both thermodynamically and kinetically to the electrochemical communication with external environments.[26] Since the coordination geometries of the diiron centers in **1c**−**4c** are not much different from one another, the spatial shielding of the diiron(III) center by the dendritic substituents is most responsible for the much lower redox activities of **3c** and **4c** (Figure 5).

Conclusions

We found that dendrimer-appended triazacyclononanes (Ln_3TACN, **2a**−**4a**) as well as nondendritic L1_3TACN (**1a**) upon reaction with $FeCl_2$ followed by NaOAc and NH_4PF_6 afford novel mononuclear iron(II) complexes ((η^2-OAc)iron(II), **1b**−**4b**), which are oxidized under O_2 to dinuclear iron(III) complexes ((μ-O)(μ-OAc)$_2$diiron(III), **1c**−**4c**). We also found that **1c**−**4c** can be reduced by photoirradiation to generate diiron(II) complexes (**1d**−**4d**), which are air-sensitive and reoxidized under O_2 to return to **1c**−**4c**. Thus, both mononuclear and dinuclear iron(II) species with dendritic TACN ligands can be generated. In particular, the diiron centers of the largest **4c** and **4d**, which are the novel spatially encumbered models of natural non-heme iron proteins, are totally encapsulated by the large dendrimer framework. Along the line of the present study, molecular design of metalloenzymes with a large dendritic cage is one of the subjects worthy of further investigation.

Experimental Section

Materials. Dichloromethane (CH_2Cl_2), washed successively with concentrated H_2SO_4, water, and aqueous $NaHCO_3$, was dried over $CaCl_2$ and distilled over CaH_2 under Ar. Ethanol (EtOH) was distilled over Mg/I_2. Tetrahydrofuran (THF) was distilled in an Ar atmosphere over sodium benzophenone ketyl just before use. Oxygen gas (O_2) was passed through silica gel, molecular sieve, and a dry ice/EtOH trap, successively. $FeCl_2 \cdot 4H_2O$ was purchased from Aldrich and used as received. $^{18}O_2$ (^{18}O, >99%) and $H_2{}^{18}O$ (^{18}O, 94%) were purchased from ISOTEC Inc. and ICON Services, respectively. Other starting materials were purchased from Tokyo Kasei Kogyo, Co., Ltd. or Wako Pure Chemicals Industries, Ltd.

Synthesis of Ln_3TACN [1a-4a (n = 1−4)]. Poly(benzyl ether) dendrimers with a triazacyclononane (TACN) focal core (Ln_3TACN, n [number of the aromatic layers] = 1−4 (**1a**−**4a**); Chart 1) were synthesized by alkaline-mediated coupling[27] of the corresponding dendron chlorides[28] with TACN, according to a method similar to that reported previously.[13] 1,4,7-Tribenzyl-1,4,7-triazacyclononane (Bn_3TACN, **Bn$_3$-1a′**) was prepared according to a literature method.[27]

Synthesis of [Fe$^{III}_2$(μ-O)(μ-OAc)$_2$(Ln_3TACN)$_2$](PF$_6$)$_2$ [1c−4c (n = 1−4)]. All operations for the synthesis of air-sensitive iron(II) complexes **1b**−**4b**, as precursors for **1c**−**4c**, were performed under Ar.

[Fe$^{III}_2$(μ-O)(μ-OAc)$_2$(L1_3TACN)$_2$](PF$_6$)$_2$ (1c). L1_3TACN (**1a**; 869.6 mg, 1.50 mmol) and $FeCl_2 \cdot 4H_2O$ (298.2 mg, 1.65 mmol) were dissolved in dry THF (30 mL), and the mixture was stirred at 20 °C overnight and then evaporated to dryness. The pale yellow residue was dissolved in dry CH_2Cl_2 (30 mL), and the solution was transferred to a flask containing a dry EtOH suspension (19 mL) of NaOAc (137.4 mg, 1.65 mmol) by means of a transfer tube through a membrane filter. The mixture was stirred for 2 h, whereupon white powder precipitated. This suspension was then transferred to a flask containing NH_4PF_6 (283.1 mg, 1.65 mmol) by means of a transfer tube through a membrane filter to remove insoluble substances. When the resulting clear solution was stirred for 2 h at room temperature, white powder precipitated. The reaction mixture was evaporated to dryness, and the residue, poured into dry CH_2Cl_2 (30 mL), was then filtered to remove insoluble substances, to give a clear yellow solution of **1b** (50 mM). After the addition of NaOAc (62.4 mg, 0.75 mmol) and NH_4PF_6 (128.7 mg, 0.75 mmol), the solution of **1b** (15 mL, 0.75 mmol) was bubbled with O_2, whereupon the reaction mixture immediately turned to a reddish-brown suspension, which was stirred overnight and then filtered. The reddish-brown solid, thus isolated, was washed with MeOH (40 mL) and dried under reduced pressure at room temperature. A $CHCl_3$ solution of the residue was exposed to ether vapor, to give **1c** as reddish-brown rectangular-shaped crystals in 55% yield (325 mg). UV−vis (MeOH): λ_{max} (nm) 351 (ϵ 12 900 cm^{-1} mol^{-1} L^{-1}), 483 (2430), 525 (1860), 722 (260). FT-IR (KBr, cm^{-1}): 1546 (ν_{sym}: μ-OAc). Raman (KCl, cm^{-1}): 514 (ν_{sym}: Fe−O−Fe), 283 (ν: Fe−N$_{trans}$). Anal. Calcd for $C_{70}H_{96}N_6F_{12}Fe_2O_{17}P_2$: C, 49.60; H, 5.71; N, 4.67. Found: C, 49.90; H, 5.87; N, 4.83. FAB-MS: 1549 ([M − PF$_6$]$^+$ calcd, 1549).

[Fe$^{III}_2$(μ-O)(μ-OAc)$_2$(L2_3TACN)$_2$](PF$_6$)$_2$ (2c). A CH_2Cl_2 solution of iron(II) complex **2b** was prepared in a manner similar to that for the preparation of **1b**. To a dry THF solution (5.0 mL) of L2_3TACN (**2a**) (83.8 mg, 0.06 mmol) was added a MeCN/THF (1/1) solution (0.44 mL) of $FeCl_2 \cdot 4H_2O$ (0.066 mmol) by a hypodermic syringe, and the mixture was stirred at 20 °C overnight and then evaporated to dryness. The pale yellow residue was dissolved in dry CH_2Cl_2 (6.0 mL), from which insoluble substances were then filtered off. EtOH solutions of NaOAc (1.32 mL, 6.6×10^{-2} mmol) and NH_4PF_6 (0.44 mL, 0.66×10^{-2} mmol) were successively added to the filtrate, and the mixture was stirred overnight and then evaporated to dryness. The pale yellow residue was dissolve in dry CH_2Cl_2 (6.0 mL), from which insoluble substances were then filtered off. To the resulting clear solution (3.0 mL) of **2b** (3.0×10^{-2} mmol) were successively added EtOH solutions of NaOAc (0.60 mL, 3.0×10^{-2} mmol) and NH_4PF_6 (0.20 mL, 3.0×10^{-2} mmol). After being bubbled with O_2 at 20 °C, the reaction mixture was stirred overnight, where the color of the solution gradually turned reddish brown. The resulting solution was evaporated to dryness, and the residue was subjected to preparative SEC, to give **2c** in 54% yield (27 mg). UV−vis ($CHCl_3$): λ_{max} (nm) 351, 482, 525, 722. FT-IR (KBr, cm^{-1}): 1548 (ν_{sym}; μ-OAc). Raman (KCl, cm^{-1}): 523 (ν_{sym}; Fe−O−Fe), 286 (ν: Fe−N$_{trans}$). Anal. Calcd for $C_{166}H_{192}N_6F_{12}Fe_2O_{41}P_2$: C, 59.89; H, 5.81; N, 2.52. Found: C, 59.88; H, 5.89; N, 2.52.

[Fe$^{III}_2$(μ-O)(μ-OAc)$_2$(L3_3TACN)$_2$](PF$_6$)$_2$ (3c). A CH_2Cl_2 solution of iron(II) complex **3b** was prepared in a manner similar to that for the preparation of **2b**. EtOH solutions of NaOAc (0.60 mL, 3.0×10^{-2} mmol) and NH_4PF_6 (0.20 mL, 3.0×10^{-2} mmol) were successively added to a CH_2Cl_2 solution (3.0 mL) of **3b** (3.0×10^{-2} mmol). After being bubbled with O_2 at 20 °C, the reaction mixture was stirred overnight, where the color of the solution gradually turned reddish brown. The resulting solution was evaporated to dryness, and the residue was subjected to preparative SEC, to give **3c** in 74% yield (73.2 mg). UV−vis ($CHCl_3$): λ_{max} 352, 482, 525, 722. FT-IR (KBr, cm^{-1}): 1548 (ν_{sym}: μ-OAc). Raman (KCl, cm^{-1}): 520 (ν_{sym}: Fe−O−Fe), 283 (ν: Fe−N$_{trans}$). Anal. Calcd for $C_{358}H_{384}N_6F_{12}Fe_2O_{89}P_2$: C, 65.18; H, 5.87; N, 1.27. Found: C, 65.32; H, 5.87; N, 1.27.

[Fe$^{III}_2$(μ-O)(μ-OAc)$_2$(L4_3TACN)$_2$](PF$_6$)$_2$ (4c). A CH_2Cl_2 solution of iron(II) complex **4b** was prepared in a manner similar to that for the preparation of **2b**. EtOH solutions of NaOAc (1.20 mL, 6.0×10^{-2} mmol) and NH_4PF_6 (0.30 mL, 4.5×10^{-2} mmol) were successively added to a CH_2Cl_2 solution (3.0 mL) of **4b** (3.0×10^{-2} mmol). After being bubbled with O_2 at 20 °C, the reaction mixture was stirred for 2 days, where the color of the solution gradually turned reddish brown. The resulting solution was evaporated to dryness, and the residue was subjected to preparative SEC, to give **4c** in 54% yield (106.5 mg). UV−

(26) A similar trend has been reported for a series of redox-active iron−sulfur clusters $[Fe_4S_4(SR)_4]^{2-}$ with poly(benzyl ether) dendritic substituents (=R). Gorman, C. B.; Parkhurst, B. L.; Su, W. Y.; Chen, K.-Y. *J. Am. Chem. Soc.* **1997**, *119*, 1141.

(27) Beissel, T.; Della Vedova, B. S. P. C.; Wieghardt, K.; Boese, R. *Inorg. Chem.* **1990**, *29*, 1736.

(28) (a) Balagurusamy, V. S. K.; Ungar, G.; Percec, V.; Johansson, G. *J. Am. Chem. Soc*. **1997**, *119*, 1539. (b) Hawker, C. J.; Fréchet, J. M. J. *J. Am. Chem. Soc*. **1990**, *112*, 7638.

vis ($CHCl_3$): λ_{max} 352, 482, 525, 722. FT-IR (KBr, cm^{-1}): 1548 (ν_{sym}: μ-OAc). Raman (KCl, cm^{-1}): 523 (ν_{sym}: Fe−O−Fe), 286 (ν: Fe−N_{trans}). Anal. Calcd for $C_{743}H_{770}N_6F_{12}Fe_2O_{184}P_2$: C, 67.97; H, 5.91; N, 0.64. Found: C, 67.90; H, 6.00; N, 0.67.

[Fe^{III}_2(μ-O)(μ-OAc)$_2$(TACN)$_2$]I_2 (1c′). **1c′** was obtained as brown solid in 24% yield from TACN (**1a′**) and $FeCl_3 \cdot 6H_2O$, according to a literature method.[21] UV−vis (MeOH): λ_{max} 336.5 nm (ϵ 6440 cm^{-1} mol^{-1} L^{-1}), 466 (960), 508.5 (770), 756.5 (180). Raman (KCl, cm^{-1}): 545 (ν_{sym}: Fe−O−Fe), 288 (ν: Fe−N_{trans}).

[Fe^{III}_2(μ-O)(μ-OAc)$_2$(Me_3TACN)$_2$](PF$_6$)$_2$ (Me_3-1c′). **Me_3-1c′** was obtained as brown solid in 33% yield from **Me_3-1a′** and $FeCl_3 \cdot 6H_2O$, according to a literature method.[22] UV−vis (MeOH): λ_{max} 346 nm (ϵ 12 800 cm^{-1} mol^{-1} L^{-1}), 474 (2240), 520 (1173), 745 (515). FT-IR (KBr, cm^{-1}): 1556 (ν_{sym}: μ-OAc). Raman (KCl, cm^{-1}): 545 (ν_{sym}: Fe−O−Fe), 288 (ν: Fe−N_{trans}). Anal. Calcd for $C_{22}H_{48}N_6F_{12}Fe_2O_5P_2$: C, 30.09; H, 5.51; N, 9.57. Found: C, 29.93; H, 5.63; N, 9.56.

[Fe^{III}_2(μ-O)(μ-OAc)$_2$(Bn_3TACN)$_2$](PF$_6$)$_2$ (Bn_3-1c′). To a CH_2Cl_2 solution (20 mL) of **Bn_3-1b′** (1.0 mmol) were added NaOAc (83.3 mg, 1.0 mmol) and NH_4PF_6 (171.6 mg, 1.0 mmol), and the mixture was stirred overnight after being bubbled with O_2 at 20 °C, where the reaction mixture immediately turned to a reddish brown suspension. Filtration of the suspension gave reddish brown solid, which was washed with MeOH (40 mL), dried under reduced pressure, and subjected to recrystallization from CH_2Cl_2/ether to give **Bn_3-1c′** as rectangular crystals in 66% yield (443.2 mg). UV−vis (MeOH): 353 nm (ϵ 10 000 cm^{-1} mol^{-1} L^{-1}), 483 (1990), 526 (1540), 731 (210). FT-IR (KBr, cm^{-1}): 1547 (ν_{sym}: μ-OAc). Raman (KCl, cm^{-1}): 520 (ν_{sym}: Fe−O−Fe), 283 (ν; Fe−N_{trans}). Anal. Calcd for $C_{58}H_{72}N_6F_{12}Fe_2O_5P_2$: C, 52.19; H, 5.44; N, 6.30. Found: C, 51.73; H, 5.41; N, 6.28.

[Fe^{III}_2(μ-^{18}O)(μ-OAc)$_2$(Bn_3TACN)$_2$](PF$_6$)$_2$ (Bn_3-[^{18}O]1c′). A CH_2Cl_2 solution of **Bn_3-1b′** (5.0×10^{-2} M, 10 mL) was added under Ar to an EtOH (10 mL) solution of a mixture of NaOAc (41.6 mg) and NH_4PF_6 (85.8 mg), and the resulting mixture was bubbled with O_2 at 20 °C just after the addition of $H_2{}^{18}O$ (100 μL). The reaction mixture was stirred overnight and then filtered under Ar to isolate reddish brown solid, which was washed with dry MeOH (10 mL) and dried under reduced pressure. **Bn_3-1b′** was obtained as reddish brown rectangular-shaped crystals in 47% yield (158.3 mg) by exposure of a CH_2Cl_2 solution of the above solid to ether vapor. Raman: ν_{sym} (Fe−^{18}O−Fe) 503 cm^{-1} (^{18}O isotope shift, −17 cm^{-1}).

Procedures. SEC Studies on Reaction of a Mixture of 1b and 3b with O_2. CH_2Cl_2 solutions of iron complexes **1b** and **3b** (10 mM, 1.00 mL) and EtOH solutions of NaOAc (0.05 M, 0.40 mL) and NH_4PF_6 (0.15 M, 0.133 mL) were successively added to an Ar-purged quartz cell of 1 mm path length, and the mixture was bubbled with O_2 and stirred at 20 °C. After 21 h, the reaction mixture was evaporated to dryness, and the residue was subjected to SEC. For a control experiment, EtOH solutions of NaOAc (0.05 M, 0.33 mL) and NH_4PF_6 (0.15 M, 0.11 mL) were successively added to a CH_2Cl_2 (1.65 mL) solution of a mixture of **1c** (6.97 mg, 4.11×10^{-3} mmol) and **3c** (27.14 mg, 4.11×10^{-3} mmol), and the resulting mixture was stirred at 20 °C for 50 h.

Kinetic Studies on Reaction of 1b−4b with O_2. To an Ar-purged quartz cell of 1 mm path length, containing a CH_2Cl_2 solution (0.80 mL) of **1b**−**4b** (10 mM), were successively added EtOH solutions of NaOAc (0.05 M, 0.16 mL) and NH_4PF_6 (0.15 M, 0.053 mL), and the cell was then placed in an EtOH bath kept at 20 °C after the introduction of O_2. Transformation of **1b**−**4b** into **1c**−**4c**, respectively, was followed by a change in absorbance at 482 nm.

Reaction of 1b with $^{18}O_2$. To an Ar-purged 100 mL flask, equipped with a three-way stopcock, containing a CH_2Cl_2 solution (12 mL) of **1b** (10 mM), were successively added EtOH solutions of NaOAc (0.05 M, 2.40 mL) and NH_4PF_6 (0.15 M, 0.80 mL). After introduction of $^{18}O_2$ to this flask, the content was stirred at 20 °C for 24 h. The reaction mixture was then evaporated to dryness, and the residue dissolved in $CHCl_3$ was chromatographed with preparative SEC, to give pure **1c** in 49% yield (49.7 mg), which was subjected to resonance Raman spectroscopy in a KCl pellet.

Photoreduction of (μ-O)(μ-OAc)$_2$Diiron(III) Complexes (1c−4c). To an Ar-purged quartz cell of 1 mm path length containing a CH_2Cl_2 solution (0.80 mL) of **1c**−**4c** (5 mM) was added an EtOH solution of NaOAc (0.05 M, 0.16 mL), and the cell, after being degassed twice by a freeze−pump−thaw method, was irradiated under Ar with a xenon arc light through a UV cutoff filter (>350 nm) at 30 °C. The characteristic absorption bands started to decay with time to give a pale yellow solution of **1d**−**4d**, where the reaction was followed by a change in absorbance at 482 nm.

EPR study on Photoreduction of 3c in the Presence of α-Phenyl-*N*-*tert*-butylnitrone (PBN). An EPR tube containing a CH_2Cl_2/EtOH (9/1) solution of a mixture of **3c** (5.0 mM), PBN (22 mM), and NaOAc (5.0 mM) was degassed by repeated freeze−pump−thaw cycles, sealed off, and then irradiated overnight at 30 °C under Ar with a xenon arc light through a UV cutoff filter (>350 nm) and subjected to EPR spectroscopy.

Reaction of 1c′, Bn_3-1c′, and 2c-4c with $H_2{}^{18}O$. The reaction of **1c′** and **Bn_3-1c′** with $H_2{}^{18}O$ was investigated according to a literature method:[4a] Dry MeCN (5 mL), distilled under Ar from P_2O_5 and then K_2CO_3, was transferred to a flask containing **1c′** (28.4 mg, 3.75×10^{-2} mmol) or **Bn_3-1c′** (50 mg, 3.75×10^{-2} mmol). To this flask was added 100 μL of $H_2{}^{18}O$ (95% enriched), and the mixture was stirred at 30 °C, from which aliquots were then periodically taken out, evaporated to dryness, and immediately subjected to FT-IR and resonance Raman spectroscopies. For **2c**, 50 μL of $H_2{}^{18}O$ was added under Ar to a dry CH_2Cl_2 solution (2.0 μM, 3.65 mL) of **2c**, and the mixture was stirred vigorously at 30 °C. After 36 h, an organic phase separated and was taken by a glass pipet and evaporated; the residue was further dried with a vacuum pump for 2 h at 40 °C. For **3c** and **4c**, 100 μL of $H_2{}^{18}O$ was used under otherwise identical conditions to the above.

Kinetic Studies on Alkaline Hydrolysis of 1c−4c. To a THF solution (0.12 mM, 2.0 mL) of [Fe^{III}_2(μ-O)(μ-OAc)$_2$(Ln_3TACN)$_2$](PF$_6$)$_2$ [**1c**−**4c** (n = 1−4)] in a quartz cell of 10 mm path length were successively added 200 μL of distilled water and 50 μL of a THF solution (3.35 M) of triethanolamine, and the mixture was kept constant at 50 °C and continuously monitored by means of UV−vis spectroscopy at 352 nm.

Measurements. Preparative size-exclusion chromatography (SEC) was performed at room temperature on a Japan Analytical Industry model LC-918 recycling preparative HPLC equipped with a variable-wavelength UV−vis detector, using $CHCl_3$ as eluent at a flow rate of 3.5 mL min^{-1}. The column set consisted of two polystyragel columns (20 [i.d.] × 600 mm [L]; JAIGEL-1H (exclusion limit: 1×10^3)/JAIGEL-2H (5×10^3) or JAIGEL-2H (5×10^3)/JAIGEL-3H (3×10^4)).

Electronic absorption spectra were recorded on a JASCO model V-570 spectrophotometer. Infrared spectra were recorded on a JASCO model FT/IR-600 Fourier transform infrared spectrometer. Resonance Raman spectroscopy was performed on a JASCO model NRS-1000 laser Raman spectrophotometer. FAB-MS spectra were recorded on a JEOL model JMS-HX110 spectrometer using a 3-nitrobenzyl alcohol matrix. EPR spectra of degassed samples were recorded at 25 °C on a JEOL FE-1X X-band spectrometer using the following parameters: magnetic field, 3280 ± 100 G; modulation, 100 kHz and 1 G; amplitude, 1; response, 0.3 s.

X-ray diffractions were collected on a MacScience DIP2000 Imaging Plate equipped with a low-temperature apparatus with graphite-monochromated Mo Kα radiation. The structural analysis was carried out with the TEXAN program package provided by Rigaku. The crystal structure of **1c** was solved using direct methods and refined with anisotropic thermal parameters for all non-hydrogen atoms. *Crystal data* for $C_{70}H_{96}F_{12}Fe_2N_6O_{17}P_2$: M = 1695.18, monoclinic, a = 14.6570(6) Å, b = 22.0010(6) Å, c = 25.0090(9) Å, β = 104.178(2)°, V = 7819.0(5) Å^3, T = 180 K, space group $P2_1/n$ (#14), Z = 4, μ(Mo K)

$= 5.09\ cm^{-1}$, 16451 reflections measured, 16005 unique ($R_{int} = 0.021$), 10293 observed ($I > 3(\sigma(I))$), and used for all calculations. The final $wR(F)$ was 0.048.

Cyclic voltammetry was performed on a BAS model CV-27 voltammetry controller at room temperature (~25 °C) with a scan speed of 100 mV s^{-1}, where diiron(III) complexes were dissolved under N_2 in MeCN (1.0×10^{-3} mM) containing Bu_4NPF_6 (0.2 M) as supporting electrolyte and ferrocene (1.0×10^{-3} mM) as internal reference. A standard three-electrode system, consisting of a Pt working electrode, a Pt auxiliary electrode, and Ag wire as pseudoreference electrode, was used. Voltage readings were referenced to a saturated calomel electrode.

Acknowledgment. We are grateful to Prof. K. Yamaguchi of Chiba University for his generous assistance of X-ray crystallographic data analysis.

Supporting Information Available: (a) SEC profiles of **1a**−**4a** and **1c**−**4c**, (b) electronic absorption spectra of **Bn$_3$-1c′** and **1c**−**4c**, (c) second-order plots of the absorption spectral changes at 482 nm of **1b**−**4b** upon reaction with O_2, (d) resonance Raman spectrum of the reaction mixture of **1b** with $^{18}O_2$, (e) resonance Raman spectrum of **Bn$_3$-1c′** and that of **Bn$_3$-[^{18}O]1c′** obtained by exposure of **Bn$_3$-1b′** to $^{16}O_2$ in the presence of $H_2{}^{18}O$, (f) differential FT-IR spectra of **2b** and **2d** obtained before and after the reaction with O_2, (g) EPR spectrum of a CH_2Cl_2/EtOH (10/1) solution of **3c** after photoirradiation in the presence of PBN, (h) SEC profile of a mixture of **1c** and **3c** after photoreduction followed by exposure to O_2, and (i) structural parameters of **1c**, summary of absorption, resonance Raman, and cyclic voltammetric data of **1c**−**4c**, **Me$_3$-1c′**, and **Bn$_3$-1c′** (PDF) and (j) crystallographic data (atomic positional and thermal parameters) of **1c** (CIF). This material is available free of charge via the Internet at http://pubs.acs.org.

JA012589N